frontiers | Frontiers in Chemistry

TYPE Original Research
PUBLISHED 19 May 2023
DOI 10.3389/fchem.2023.1199863

OPEN ACCESS

EDITED BY
Wei Zeng,
Tohoku University, Japan

REVIEWED BY
Bogdan M Benin,
Northeast Ohio Medical University, United States
Lin Wang,
Shanghai University, China

*CORRESPONDENCE
Minqiang Wang,
mqwang@xjtu.edu.cn

RECEIVED 04 April 2023
ACCEPTED 11 May 2023
PUBLISHED 19 May 2023

CITATION
Zhang C, Wang M, Shi J, Wang J, Da Z, Zhou Y, Xu Y, Gaponenko NV and Bhatti AS (2023), Preparation of $CsPb(Cl/Br)_3/TiO_2:Eu^{3+}$ composites for white light emitting diodes.
Front. Chem. 11:1199863.
doi: 10.3389/fchem.2023.1199863

Preparation of $CsPb(Cl/Br)_3/TiO_2:Eu^{3+}$ composites for white light emitting diodes

Chen Zhang[1], Minqiang Wang[1]*, Jindou Shi[1], Junnan Wang[1], Zheyuan Da[1], Yun Zhou[1], Youlong Xu[1], Nikolai V. Gaponenko[2] and Arshad Saleem Bhatti[3]

[1]Electronic Materials Research Laboratory, Key Laboratory of the Ministry of Education International Center for Dielectric Research and Shannxi Engineering Research Center of Advanced Energy Materials and Devices, Xi'an Jiaotong University, Xi'an, China, [2]Belarusian State University of Informatics and Radioelectronics, Minsk, Belarus, [3]Centre for Micro and Nano Devices, Department of Physics, COMSATS Institute of Information Technology, Islamabad, Pakistan

The inherent single narrow emission peak and fast anion exchange process of cesium lead halide perovskite $CsPbX_3$ (X = Cl, Br, I) nanocrystals severely limited its application in white light-emitting diodes. Previous studies have shown that composite structures can passivate surface defects of NCs and improve the stability of perovskite materials, but complex post-treatment processes commonly lead to dissolution of NCs. In this study, $CsPb(Cl/Br)_3$ NCs was in-situ grown in TiO_2 hollow shells doped with Eu^{3+} ions by a modified thermal injection method to prepare $CsPb(Cl/Br)_3/TiO_2:Eu^{3+}$ composites with direct excitation of white light without additional treatment. Among them, the well-crystalline TiO_2 shells acted as both a substrate for the dopant, avoiding the direct doping of Eu^{3+} into the interior of NCs to affect the crystal structure of the perovskite materials, and also as a protection layer to isolate the contact between PL quenching molecules and NCs, which significantly improves the stability. Further, the WLED prepared using the composites had bright white light emission, luminous efficiency of 87.39 lm/W, and long-time operating stability, which provided new options for the development of perovskite devices.

KEYWORDS

$CsPb(Cl/Br)_3/TiO_2:Eu^{3+}$, perovskite, anatase, nano-materials, white light emitting diodes

1 Introduction

Cesium lead halide perovskite $CsPbX_3$ (X = Cl, Br, I) nanocrystals (NCs) has attracted a lot of attention from researchers due to its excellent optoelectronic properties and versatile surface chemistry (Tang et al., 2016; Zhou et al., 2016; Pan et al., 2018a). White light-emitting diodes (WLEDs) prepared by $CsPbX_3$ NCs have high luminous efficiency and low energy consumption, making them one of the favorable candidates for next-generation photoelectric devices (Dai et al., 2014; Pan et al., 2016; Yang et al., 2019). However, if the light-emitting layer of WLED were to use both $CsPbI_3$, $CsPbBr_3$ and $CsPbCl_3$ as RGB light sources would inevitably lead to impure chromaticity due to anion exchange between halogenated elements (Zhang et al., 2017; Shi et al., 2022). Meanwhile, the problem of instability of $CsPbX_3$ NCs in working environment also impeded its further development in the fields of display and lighting (Yang et al., 2015; Shi et al., 2019; Shi et al., 2020; He et al., 2022).

Currently, the mainstream method of combining white light by $CsPbX_3$ NCs was achieved by mixing NCs with other phosphors or doping with other luminophor. For example, Yuan et al. sensitized $CsPbI_3$ NCs by doping with Yb^{3+} ions, mixed them with $Y_3Al_5O_{12}$:Ce^{3+} green phosphors, and integrated them on GaN blue LED chips to finally prepare WLED with good stability (Yuan et al., 2020). Pan et al. (2017) prepared $CsPbCl_3$ NCs with Ln^{3+} ion (Ce^{3+}、Sm^{3+}、Eu^{3+}、Dy^{3+}、Er^{3+}, and Yb^{3+}) emission peaks by doping Ln^{3+} ions into the lattice of $CsPbCl_3$ NCs. In a subsequent study, they further doped the $CsPb(Cl/Br)_3$ NCs with lanthanide ion pairs (Ce^{3+}/Mn^{2+}、Ce^{3+}/Eu^{3+}, and Ce^{3+}/Sm^{3+}) to achieve white phosphors with 75% high photoluminescence quantum yields (PLQY) (Pan et al., 2018b). However, due to the environmentally sensitive nature of $CsPbX_3$ NCs, the low efficiency of the prepared LEDs and the instability of the phosphors in each layer were still to be solved (Bae et al., 2013; Fakharuddin et al., 2019). Meanwhile, when the doping ions entered the interior of the $CsPbX_3$ NCs lattice, it inevitably influenced the crystal structure of $CsPbX_3$ NCs, resulting in the shift of the NCs luminescence wavelength (Huang et al., 2022). Therefore, it is necessary to develop highly efficient and stable composite materials that can directly excite white light.

In this paper, we propose a convenient synthetic strategy to prepare $CsPb(Cl/Br)_3/TiO_2:Eu^{3+}$ composites which can directly excite white light. The pre-prepared TiO_2 hollow shells were placed in the precursor solution and $CsPb(Cl/Br)_3$ NCs were in-situ grown inside the shells by thermal injection method. Among it, the pre-prepared TiO_2 hollow shells acted as hosts for Eu^{3+} ions with bright red light emission (~614 nm), which both avoided the change of the perovskite crystal structure caused by direct doping and replaced the $CsPbI_3$ NCs, solving the problem of anion exchange due to the introduction of I^-. Further, the stability of the NCs was significantly improved benefited from the protection of the external TiO_2 hollow shells. The WLEDs prepared using $CsPb(Cl/Br)_3/TiO_2:Eu^{3+}$ composites exhibited a luminous efficiency of 87.39 lm/W and long-time operating stability, which greatly enhances the potential competitiveness of perovskite materials for commercial lighting device applications.

2 Materials and methods

2.1 Materials

The cesium carbonate (Cs_2CO_3, 99.99%), lead (II) bromide ($PbBr_2$, 99.99%), lead (II) chloride ($PbCl_2$, 99.99%), oleic acid (OA, 85%), oleylamine (OAm, 80–90%), 1-octadecene (ODE, 90%), Tetrabutyl titanate (TBOT, >99%) and Tetraethyl orthosilicate (TEOS, >99%) were purchased from Aladdin. Europium (III) nitrate hexahydrate ($Eu(NO_3)_3{\cdot}6H_2O$, 99.9%) and isopropyl alcohol (IPA, Analytical Reagent) were purchased from Macklin. The poly (styrene) (PS), ethanol absolute (Analytical Reagent), ammonia solution (NH_4OH) and toluene (>99.5%) purchased from Shanghai Chemical Industrial Company. The 365 nm UV-chips (10W) and commercial WLED (10W) were purchased from Shenzhen Youjing Optoelectronics factory. All the reagents were used without further purification.

2.2 Synthesis of $TiO_2:Eu^{3+}$ hollow shells

5 mL TEOS was slowly added to the mixture of 0.35 mL NH_4OH, 2.5 mL deionized water and 20 mL IPA and stirred continuously at room temperature for 5 h to obtain SiO_2 by hydrolysis. After that, the crude product was centrifuged at 3,000 rpm/min for 5 min to obtain white precipitates, washed several times with deionized water, and dried at 60°C for 12 h to obtain SiO_2 spherical templates with average particle size of 340 nm.

0.25 g SiO_2 spherical templates and 0.2–1.2 mmol europium acetate were placed into the mixed solution of 0.75 mL deionized water and 37.5 mL ethanol, and sonicated for 20 min to make them completely dispersed. After that, 1.25 mL TBOT were slowly dropped into the mixed solution and stirred for 5 h at room temperature to make it completely hydrolyzed. The products were annealed at 800°C for 3 h to obtain $SiO_2/TiO_2:Eu^{3+}$ composites (The heating rate was 100°C/h). Finally, the composites were etched in ammonia at concentration of 4 M for 14 h until the SiO_2 spheres disappeared completely, and the secondary annealing was performed under the same conditions to obtain $TiO_2:Eu^{3+}$ hollow shells.

2.3 Synthesis of the $CsPb(Cl/Br)_3/TiO_2:Eu^{3+}$ composites

0.814 g Cs_2CO_3 were placed in the mixture of 2.5 mL OA and 10 mL ODE and transferred to a 100 mL three-neck flask. The solution was heated to 120 °C under vacuum for 1 h. After that, the solution was heated to 140 °C under N_2 for another 1 h to obtain the Cs-OA precursor. Cs-OA precursors required to be held at 100 °C before use.

0.1 mmol of $PbCl_2$ and $PbBr_2$ ($PbCl_2$:$PbBr_2$ was 9:1, 2:1, 1:1, 1:2 and 1:9, respectively), 0.3 g $TiO_2:Eu^{3+}$ hollow shells were placed in the mixture consisting of 10 mL ODE, 0.5 mL OA and 0.5 mL OAm and transferred to another 100 mL three-neck flask. After warming to 120 °C for 1 h under N_2, the reaction was then warmed to 150 °C for 10 min, and then 0.6 mL Cs-OA were injected into the solution. After 5–10 s, the reaction was terminated by immersing the three-necked flask in ice water. The solution was continued to stir at room temperature for 1 h to grow NCs in $TiO_2:Eu^{3+}$ hollow shells. The crude solution was centrifuged at 2000 rpm/min for 5 min to obtain the precipitate, and washed with toluene 2–3 times. The obtained product was dried under vacuum at 60°C for 5 h to obtain $CsPb(Cl/Br)_3/TiO_2:Eu^{3+}$ composites.

2.4 Preparation of WLEDs

First, 0.05 g $CsPb(Cl/Br)_3/TiO_2:Eu^{3+}$ powders and 0.5 g PS particles were placed in 5 mL toluene and stirred at 60°C for 3 h. Then, the solution was poured into prefabricated molds and $CsPb(Cl/Br)_3/TiO_2:Eu^{3+}$ polymer films were deposited at room temperature. Finally, films were coated on a 365 nm UV-chip to obtain LEDs with white light emission.

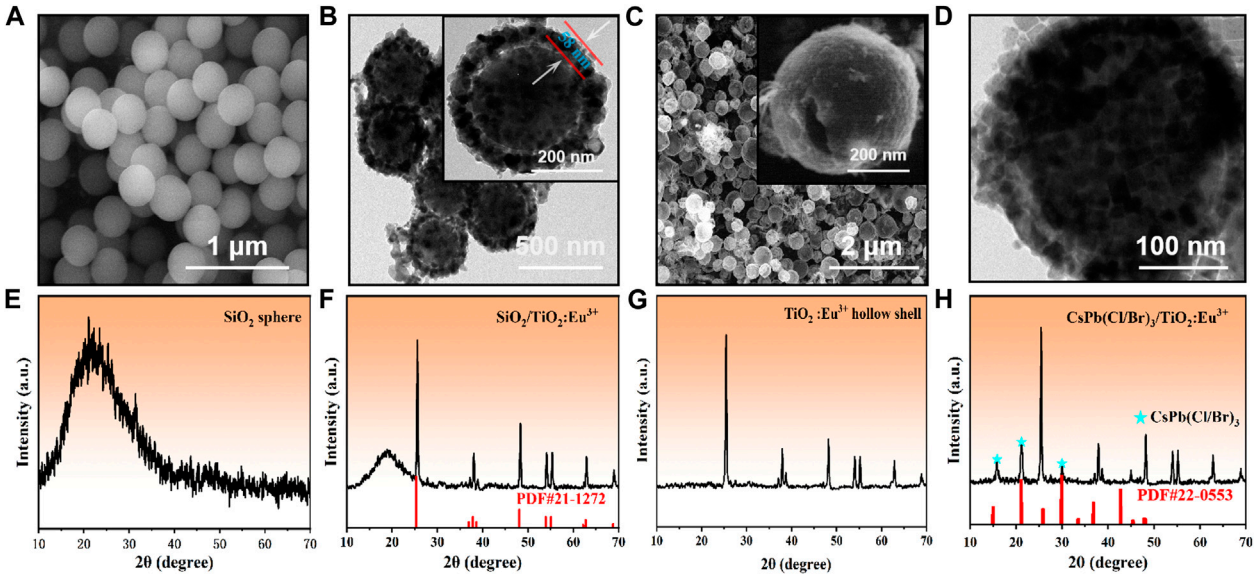

FIGURE 1
(A, E) SEM images and XRD patterns of SiO_2 nanoparticles. **(B, F)** TEM images and XRD patterns of SiO_2/TiO_2:Eu^{3+} composites. **(C, G)** SEM and XRD patterns of TiO_2:Eu^{3+} hollow shells. **(D, H)** TEM images and XRD patterns of $CsPb(Cl/Br)_3/TiO_2$:Eu^{3+} composites. The doping amount of Eu^{3+} ions in this part of the sample was 0.6 mmol, and the annealing temperature was 800°C.

2.5 Characterization

The morphology and microstructure of the samples were analyzed by transmission electron microscope (TEM, JEOL JEM-F200). The energy dispersive spectroscopy (EDS) spectra of the SiO_2/TiO_2:Eu^{3+} powder samples were investigated with field emission scanning electron microscope (SEM, FEI Quatan FEG 250) equipped EDS. Photoluminescence (PL) spectra and time-resolved PL (TRPL) decay curves of the samples were recorded on Edinburgh Instruments FLS1000 spectrometer. UV-Vis absorption spectra were recorded with the Jasco V-570 UV/VIS/NIR spectrophotometer. The X-ray diffraction (XRD) patterns were obtained with the DB-ADVANCE X-ray diffractometer. Electroluminescence (EL) spectra of white LEDs were collected by a Keithley 2,400 light source meter and the Photo Research 670 spectrometer.

3 Results and discussion

3.1 Preparation process of $CsPb(Cl/Br)_3/TiO_2$:Eu^{3+} composites

In this paper, $CsPb(Cl/Br)_3/TiO_2$:Eu^{3+} composites with multi-peak emission were obtained by a two-step method (Supplementary Figure S1). First, we synthesized a series of monodisperse SiO_2 spheres as nanotemplates for the preparation of TiO_2 hollow shells. The pre-prepared SiO_2 nanoparticles exhibited uniform size (approximately 340 nm) and smooth surface, which are ideal template materials (Figure 1A; Supplementary Figures S2A, B). Afterwards, SiO_2/TiO_2:Eu^{3+} composites were obtained by TBOT hydrolysis and annealed at high temperature. The energy dispersive spectroscopy (EDS) showed that the Ti elements were uniformly distributed on the surface of the SiO_2 spheres, forming mesoporous TiO_2 shells (Supplementary Figure S3). The average size was approximately 460 nm, and the shell thickness was approximately 58 nm (Figure 1B; Supplementary Figures S2C, D). The corresponding XRD results showed two characteristic diffraction peaks for amorphous SiO_2 and anatase TiO_2 (PDF#21-1272) (Figure 1F), and no other impurity phases appeared, attributed to the low doping concentration of Eu^{3+} ions in the surface TiO_2 layer. Further, a series of hollow TiO_2:Eu^{3+} shells were obtained by using ammonia to, etch the SiO_2 templates (Figure 1C) (Chang et al., 2017). The inset showed the surface pores of the TiO_2:Eu^{3+} hollow shells, which can ensure the smooth entry and crystallization of Cs^+, Pb^{2+}, Cl^- and Br^- ions from the solution into the shells. At this time, the XRD pattern also showed that the broad peak of amorphous SiO_2 had completely disappeared (Figure 1G), which proved that the SiO_2 template could be effectively removed by prolonged etching with ammonia. The corresponding EDS spectra showed that the Eu^{3+} ions were uniformly distributed in the TiO_2 hollow shells without agglomeration (Supplementary Figure S4). Finally, $CsPb(Cl/Br)_3$ NCs were grown *in situ* in TiO_2:Eu^{3+} hollow shells to obtain $CsPb(Cl/Br)_3/TiO_2$:Eu^{3+} composites. Most of the $CsPb(Cl/Br)_3$ NCs have entered the TiO_2:Eu^{3+} hollow shells as observed by TEM images (Figure 1D), and the XRD pattern of this materials (Figure 1H) showed the diffraction peaks of $CsPb(Cl/Br)_3$ NCs (PDF#22-0553) in addition to the diffraction peaks of anatase phase TiO_2, which indicated that both had completed the composite. In summary, the formation process of $CsPb(Cl/Br)_3/TiO_2$:Eu^{3+} was demonstrated by SEM, TEM and XRD variations, which confirmed that the composites could be successfully obtained by a simple two-step method.

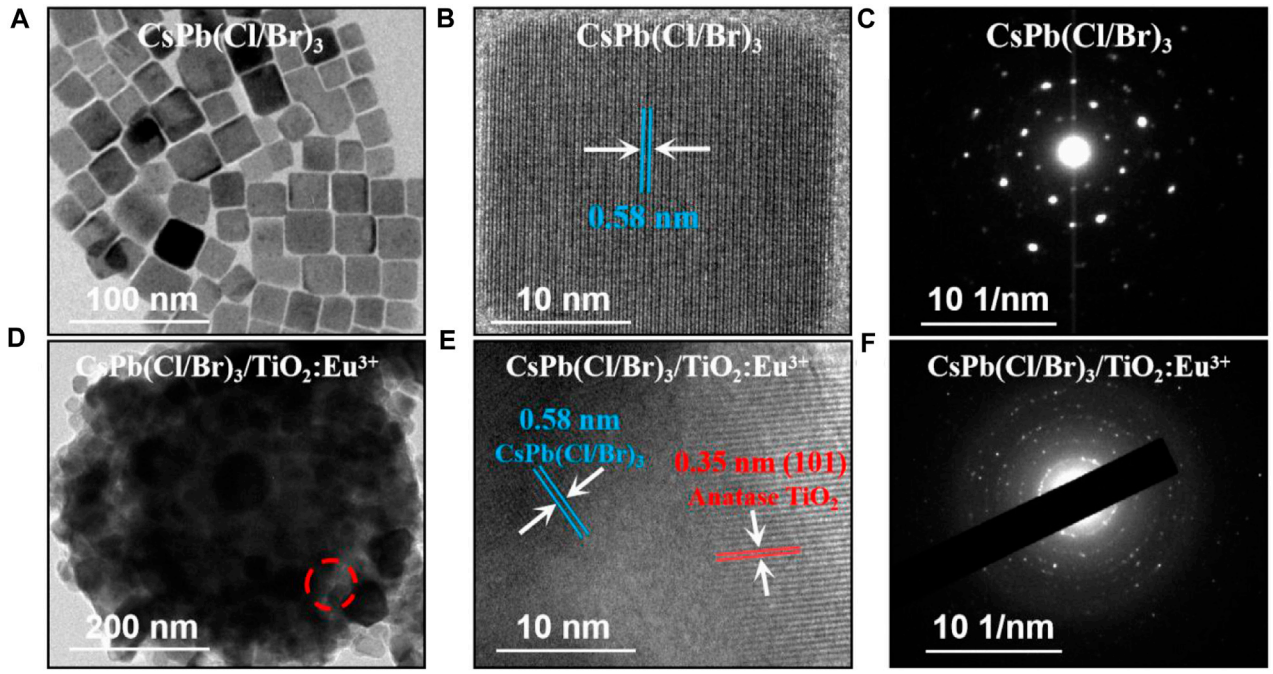

FIGURE 2
(A) TEM, **(B)** HRTEM and **(C)** SAED images of CsPb $(Cl/Br)_3$ NCs. **(D)** TEM, **(E)** HRTEM at the position of the red circle and **(F)** SAED images of CsPb $(Cl/Br)_3/TiO_2:Eu^{3+}$ composites.

3.2 $CsPb(Cl/Br)_3$ and $CsPb(Cl/Br)_3/TiO_2:Eu^{3+}$ crystal structures

Subsequently, the microscopic morphology and crystal structure of $CsPb(Cl/Br)_3$ NCs and $CsPb(Cl/Br)_3/TiO_2:Eu^{3+}$ composites were further analyzed. First, the pure $CsPb(Cl/Br)_3$ NCs had average size of approximately 26 nm and had good dispersion (Figure 2A; Supplementary Figures S2E, F). The corresponding high-resolution transmission electron microscopy (HRTEM) images showed clear lattice stripes with crystal plane spacing of about 0.58 nm (Figure 2B). Selected area electron diffraction (SAED) images were typical of single-crystal diffraction spots, indicating that the prepared $CsPb(Cl/Br)_3$ NCs have good crystallinity (Figure 2C) (Song et al., 2015; Yan et al., 2020). Similarly, the $CsPb(Cl/Br)_3/TiO_2:Eu^{3+}$ composites were observed by TEM and many cubic $CsPb(Cl/Br)_3$ NCs were found to be encapsulated within $TiO_2:Eu^{3+}$ hollow shells (Figure 2D). Afterwards, two lattice fringes with different spacing could be clearly observed at the red circle in Figure 2D, corresponding to $CsPb(Cl/Br)_3$ NCs (spacing 0.58 nm) and the $TiO_2:Eu^{3+}$ hollow shells [spacing 0.35 nm, anatase (101) crystalline surface] (Figure 2E). Also, the multilayer ring-like SAED images further verified the excellent crystallinity of the composites (Figure 2F) (Dong et al., 2021).

3.3 Optical properties of $TiO_2:Eu^{3+}$ hollow shells

In order to make the materials emit white light directly, it is necessary to match the fluorescence intensity of different light sources. However, compared with the high quantum yield of $CsPbX_3$ NCs, the excitation light of Eu^{3+} ions was often hidden (Wang et al., 2017; Shi et al., 2021; Xu et al., 2022). Therefore, the effects of the concentration of Eu^{3+} ions and annealing temperature were investigated in this paper to make the $TiO_2:Eu^{3+}$ hollow shells showing the brightest red light emission. First, the TiO_2 hollow shell samples with different doping amounts were white powders under daylight, but emitted different intensities of red light under 365 nm UV excitation (Supplementary Figure S5A). Clearly, the 0.6 mmol doped sample had the brightest red light effect. The corresponding PL spectra proved this point (Supplementary Figure S5B), and the PL intensity began to decrease with further increase of doping amount. This phenomenon was attributed to the concentration quenching effect, where the central distance between ions gradually decreases as the concentration of Eu^{3+} ions increases, leading to an increase in the cross-relaxation rate, which adversely affects the fluorescence intensity (Gao et al., 2021). Meanwhile, the XRD results indicated that the PL intensity decrease was also related to the phase change of the TiO_2 host. High concentration (0.8 mmol and above) of Eu^{3+} doping converted anatase TiO_2 to $Eu_2Ti_2O_7$ (PDF#23-1072) and rutile TiO_2 (PDF#21-1276) (Supplementary Figure S5C). However, due to the highly symmetric crystal structure of $Eu_2Ti_2O_7$, the products had non-PL activity (Mrázek et al., 2015; Orihashi et al., 2016). Thus, the concentration quenching effect and the substrate phase transition both together lead to the decay of the emission intensity of $TiO_2:Eu^{3+}$ hollow shells above 0.8 mmol. Through Rietveld refinement of XRD data, the content of each phase in the product at this time was calculated to determine the conversion rate of anatase (Supplementary Figure S6). The results showed that 73.2% of the anatase TiO_2 substrate

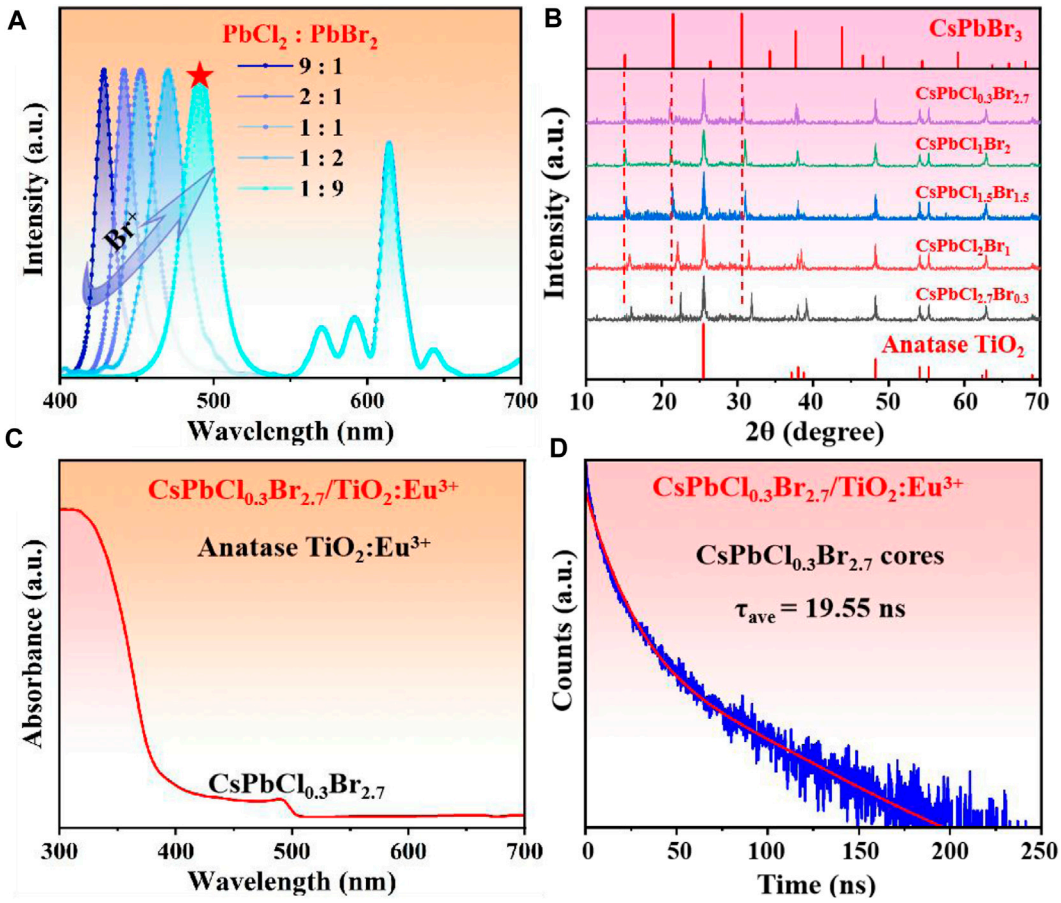

FIGURE 3
(A) PL spectra (λ_{em} = 365 nm) and **(B)** XRD patterns of $CsPb(Cl/Br)_3/TiO_2:Eu^{3+}$ composites with different Cl/Br ratios. **(C)** Absorption spectra and **(D)** time-resolved fluorescence spectra of $CsPbCl_{0.3}Br_{2.7}/TiO_2:Eu^{3+}$ composites (monitoring peak at 491 nm). The Eu^{3+} ion doping concentration of all samples was 0.6 mmol and the annealing temperature was 800°C.

underwent phase transformation, among which rutile accounted for 33.2% of the total and $Eu_2Ti_2O_7$ was 40.0%. Therefore, precise control of the Eu^{3+} ion doping ratio was crucial. In addition, the main peaks of both the anatase TiO_2 and $Eu_2Ti_2O_7$ were slightly shifted in the small-angle direction as the Eu^{3+} doping in the TiO_2 host increased, attributed to the replacement of the smaller Ti^{4+} (61 p.m.) by the larger ionic radius Eu^{3+} (94.7 p.m.) (Supplementary Figure S5C) (Pan et al., 2017). Consistent results were also observed in the UV-Vis absorption spectra (Supplementary Figure S5D), confirming that the increase of Eu^{3+} doping would lead to the rapid transformation of anatase TiO_2 to $Eu_2Ti_2O_7$. In summary, the 0.6 mmol Eu^{3+} ion doped TiO_2 has both no impurity generation and the strongest red light emission.

Similarly, the annealing process was an essential step for the formation of highly crystalline $TiO_2:Eu^{3+}$ hollow shells and played a decisive role in the optical properties of the Eu^{3+} ions (Werts et al., 2002; Reszczyńska et al., 2016). We further investigated the effect of temperature on the fluorescence intensity of $TiO_2:Eu^{3+}$ hollow shells. The PL spectra showed that the emission intensity of samples peaked at 800°C (Supplementary Figure S7A). The XRD results revealed the reason for the fluorescence change (Supplementary Figure S7B). The diffraction peaks of anatase TiO_2 gradually became stronger at 600–800°C, especially the sharp diffraction peaks at 800°C indicated that the $TiO_2:Eu^{3+}$ hollow shells had the best crystallinity at this time. However, when the annealing temperature rises to 900°C, the products showed a transformation similar to the previous results (from anatase to rutile and $Eu_2Ti_2O_7$). It was concluded that at the 600–800°C range, the increased annealing temperature resulted in a better crystallinity of the TiO_2 host and lower density of defect states between the grains, leading to stronger fluorescence emission (Ningthoujam et al., 2009; Chang et al., 2017). When the temperature was further increased (900°C), the sub-stable anatase TiO_2 reacted with Eu^{3+} ions free inside the lattice to form $Eu_2Ti_2O_7$, leading to a decrease in fluorescence intensity. The XRD results of $TiO_2:Eu^{3+}$ hollow shells at low temperatures (300–500°C) showed no or very low diffraction peaks, indicating that the lowest temperature to make hollow shells crystallize was 500°C (Supplementary Figure S8). In addition, we also compared the phase transition process of pure TiO_2 at different annealing temperatures and found that the anatase to rutile transition occurred at 800°C (Supplementary Figures S9A, B). This

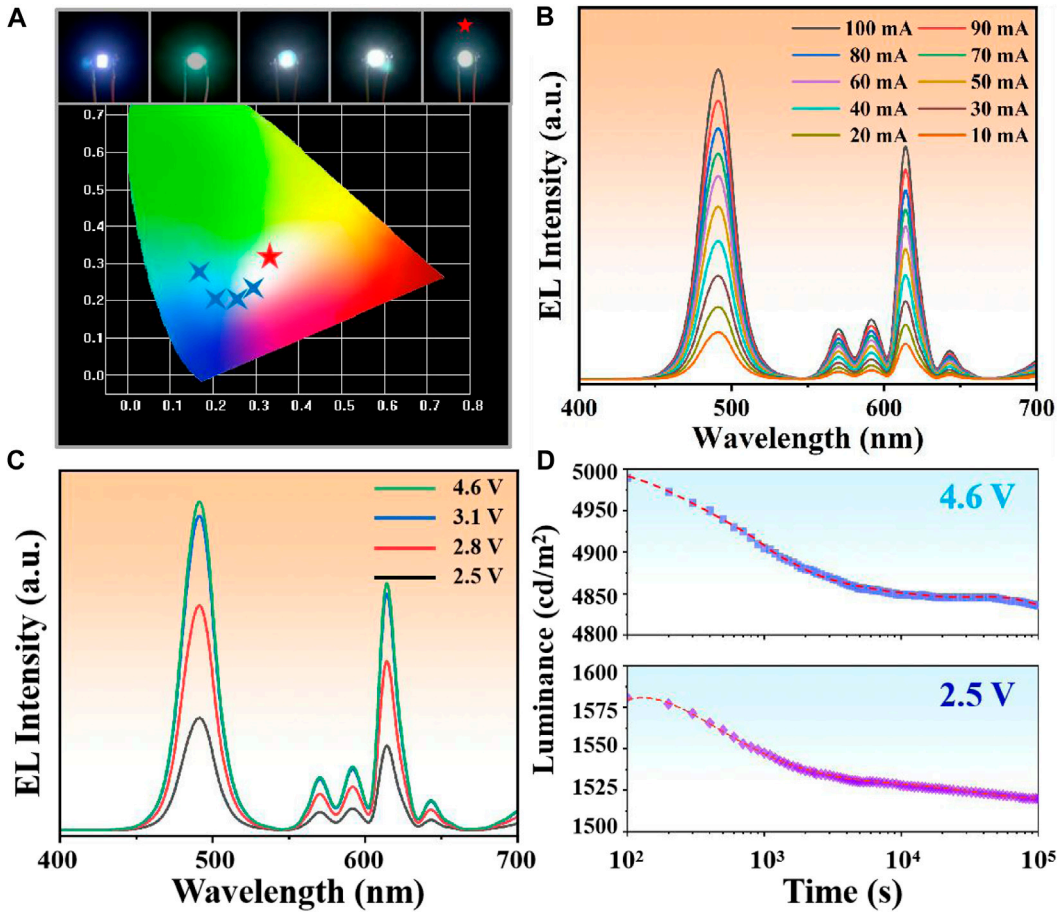

FIGURE 4
(A) Chromaticity coordinates of LEDs prepared from composites with different Cl/Br ratios. Among them, $CsPbCl_{0.3}Br_{2.7}/TiO_2:Eu^{3+}$ WLED showed the purest white light emission (0.318, 0.326). **(B)** EL spectra of $CsPbCl_{0.3}Br_{2.7}/TiO_2:Eu^{3+}$ WLED at 10–100 mA drive current. **(C)** EL spectra of $CsPbCl_{0.3}Br_{2.7}/TiO_2:Eu^{3+}$ WLED at different drive voltages. **(D)** Stability fitting curves of $CsPbCl_{0.3}Br_{2.7}/TiO_2:Eu^{3+}$ WLED at 2.5 V and 4.6 V.

phenomenon proved that the doping of Eu^{3+} ions could stabilize the crystal structure of anatase TiO_2 and make it withstand higher temperatures without phase transformation. Subsequently, the optical properties of $TiO_2:Eu^{3+}$ hollow shells at different annealing temperatures were further investigated. The corresponding UV-Vis absorption spectra showed that the absorption edge of the samples appeared to change significantly when the temperature was increased to 900°C (Supplementary Figure S7C), which was another proof that high temperature induced the transformation of TiO_2 to $Eu_2Ti_2O_7$. Meanwhile, the time-resolved fluorescence spectra showed that the average lifetimes of Eu^{3+} ions in TiO_2 hollow shells were 80.32, 106.54, 193.69, and 131.27 μs at 600, 700, 800°C, and 900°C, respectively (Supplementary Figure S7D). Among them, the $TiO_2:Eu^{3+}$ hollow shells at 800°C showed the longest average lifetimes, which proved that the increased crystallinity was beneficial to suppress the nonradiative recombination and thus improved the luminescence efficiency of Eu^{3+} ions. In summary, the $TiO_2:Eu^{3+}$ hollow shells annealed at 800°C exhibited the best crystallinity and fluorescence emission and were used as the source of red light emission in WLED.

3.4 Optical properties of $CsPb(Cl/Br)_3/TiO_2:Eu^{3+}$ composites

Subsequently, we had in-situ grown $CsPb(Cl/Br)_3$ NCs inside TiO_2 hollow shells to obtain composites with direct white light emission. It has been known that white light composed of multi-color light, which required multiple light sources to cooperate to achieve the emission. First, We synthesized a series of $CsPb(Cl/Br)_3/TiO_2:Eu^{3+}$ composites with different Cl/Br ratios to match the red light (~614 nm) of $TiO_2:Eu^{3+}$ hollow shells to obtain pure white light. The pictures of the samples showed that the phosphor gradually changed from blue emission to white as the Br^- concentration increased (Supplementary Figure S10A). The corresponding PL spectra (Figure 3A) showed that multiple emission peaks were present for all samples, corresponding to the $CsPb(Cl/Br)_3$ NCs (before 500 nm) and the Eu^{3+} ions (after 500 nm). Both characteristic peaks of anatase TiO_2 and $CsPb(Cl/Br)_3$ NCs were also present in the XRD patterns of the samples (Figure 3B). Moreover, the diffraction peaks of NCs shifted toward large angles with increasing Cl^- ion content, which was attributed to the replacement of larger Br^- by Cl^- with smaller ionic radius

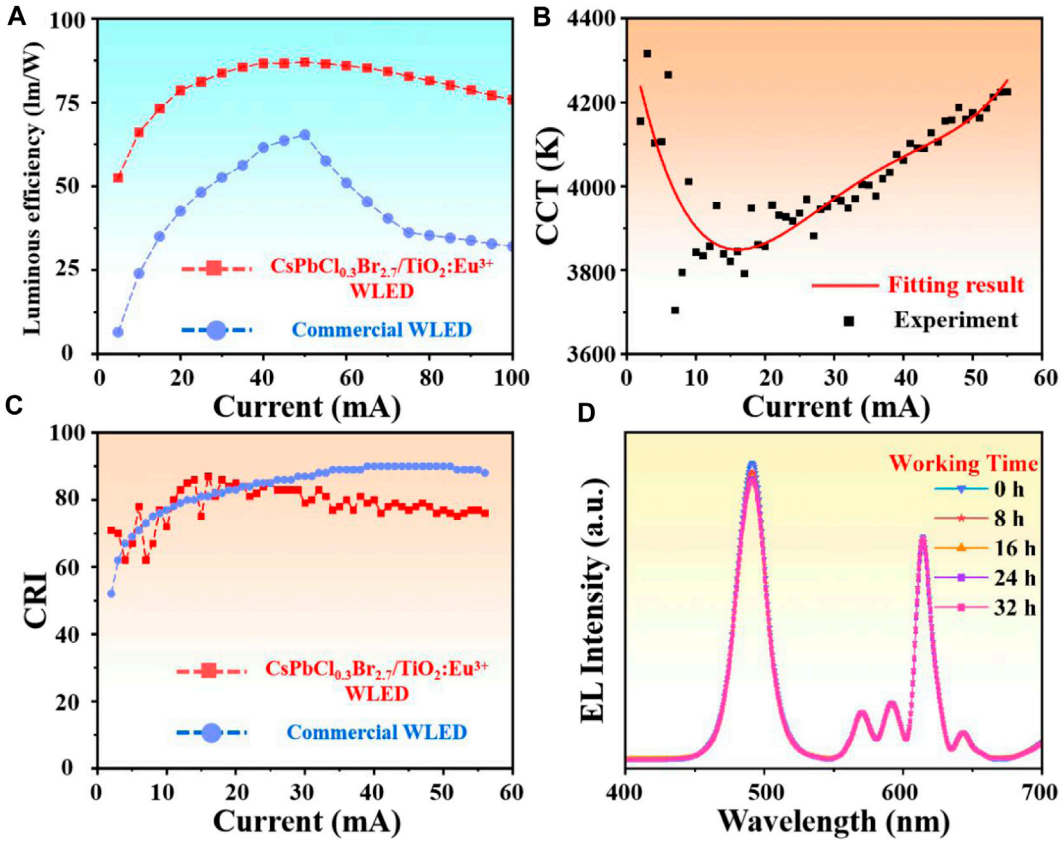

FIGURE 5
(A) Comparison of the luminous efficiency of $CsPbCl_{0.3}Br_{2.7}/TiO_2:Eu^{3+}$ WLED and commercial WLED. **(B)** The correlated color temperatures of $CsPbCl_{0.3}Br_{2.7}/TiO_2:Eu^{3+}$ WLED at 2–60 mA drive current. **(C)** Comparison of the color rendering index of $CsPbCl_{0.3}Br_{2.7}/TiO_2:Eu^{3+}$ WLED and commercial WLED. **(D)** EL spectra of $CsPbCl_{0.3}Br_{2.7}/TiO_2:Eu^{3+}$ WLED operating continuously for 32 h at 20 mA drive current.

(Protesescu et al., 2015; Bai et al., 2022). Subsequently, the absorption spectrum of $CsPbCl_{0.3}Br_{2.7}/TiO_2:Eu^{3+}$ with the best white light effect was tested (Figure 3C), where the absorption peak at 490 nm was assigned to $CsPb(Cl/Br)_3$ NCs and the absorption peak before 400 nm to $TiO_2:Eu^{3+}$ hollow shells. Further, we monitored the fluorescence lifetime of $CsPbCl_{0.3}Br_{2.7}/TiO_2:Eu^{3+}$ composites and pure phase $CsPbCl_{0.3}Br_{2.7}$ NCs at 491 nm to demonstrate the passivation effect of $TiO_2:Eu^{3+}$ hollow shells (Figure 3D). The results showed that the average lifetime of $CsPb(Cl/Br)_3/TiO_2:Eu^{3+}$ composites was 19.55 ns, while the pure $CsPbCl_{0.3}Br_{2.7}$ NCs was only 10.52 ns (Supplementary Figure S10B). The significant extension of the lifetime of NCs proved that the $TiO_2:Eu^{3+}$ shell layer can effectively isolate the PL quenching molecules from entering the interior and avoided the increase in the density of defect states on the surface of NCs by the external environment, thus improving the radiative recombination efficiency (Ravi et al., 2020; Ji et al., 2021). Finally, we compared the stability of the composites and pure phase $CsPbCl_{0.3}Br_{2.7}$ NCs, and the results were shown in Supplementary Figure S11. First, after 5 h of immersion in water, the $CsPbCl_{0.3}Br_{2.7}/TiO_2:Eu^{3+}$ could retain 72% of the fluorescence intensity, and the $CsPbCl_{0.3}Br_{2.7}$ NCs were 55% (Supplementary Figures S11A, B). The fluorescent intensity of both materials was dramatically reduced, attributed to external water molecules that could diffuse to the interior through the surface pores of the hollow shells, resulting in no appreciable improvement in water stability. However, the test results of thermal stability were surprising. After continuous heating at 80°C, the composites could still maintain more than 90% of PL intensity, while the $CsPbCl_{0.3}Br_{2.7}$ NCs had been mostly quenched (Supplementary Figures S11C, D). The light stability also exhibited similar results, demonstrating that the TiO_2 shells can isolate some of the PL quenching molecules, allowing the perovskite NCs to maintain the stability of the crystal structure while withstanding more severe environmental aggression (Supplementary Figures S11E, F). Therefore, all the above results demonstrated that the $CsPbCl_{0.3}Br_{2.7}/TiO_2:Eu^{3+}$ composites had efficient white light emission and excellent stability.

3.5 Preparation and performance of WLEDs

As one of the most important applications of $CsPbX_3$ NCs, the luminous efficiency and stability of LED determined the development prospect of the materials (Dong et al., 2020; Yoon et al., 2023). We prepared a series of LEDs by encapsulating composites with polymers (Polystyrene) and integrating them onto 365 nm chips. Among them, the $CsPbCl_{0.3}Br_{2.7}/TiO_2:Eu^{3+}$ LED exhibited the purest white light emission (0.318, 0.326)

(Figure 4A), which was consistent with the observation of the previous samples. Further, the EL spectra at different drive currents (Figure 4B) and different drive voltages (Figure 4C) showed that the WLED peak positions were not shifted, demonstrating the good luminous stability of the device. The time-dependent EL decay curve of $CsPbCl_{0.3}Br_{2.7}/TiO_2:Eu^{3+}$ WLED (Figure 4D) showed that the luminous intensity of WLED had a fast decaying trend (decaying about 2–3%) in the first 1,000 s at either high voltage (4.6 V) or low voltage (2.5 V), and then tends to level off. This phenomenon was attributed to the rapid heating of the device surface, which caused thermal decomposition of the NCs unshielded by the TiO_2 shells. However, after reaching thermal equilibrium (>1,000 s), the decay trend slows down by two orders of magnitude, demonstrating that the TiO_2 shells isolated the external thermal environment, and effectively decelerated the decomposition rate of NCs.

Subsequently, the highest luminous efficiency of $CsPbCl_{0.3}Br_{2.7}/TiO_2:Eu^{3+}$ WLED was 87.39 lm/W, which was approximately 38.4% higher than commercial WLED (Maximum about 63.14 lm/W) (Figure 5A). Such high luminescence efficiency was attributed to the effective passivation of NCs surface defects by the external highly crystalline $TiO_2:Eu^{3+}$ hollow shells. Moreover, the correlated color temperature (CCT) fluctuated from 3,700 to 4,300 K with a warm white color, which can effectively avoid the damage of blue light to human eyes (Figure 5B) (Fan et al., 2023; He et al., 2023; Yang et al., 2023). Figure 5C exhibited the color rendering index (CRI) comparison between $CsPbCl_{0.3}Br_{2.7}/TiO_2:Eu^{3+}$ WLED and commercial WLED. The results indicated that the CRI of $CsPbCl_{0.3}Br_{2.7}/TiO_2:Eu^{3+}$ WLED remained above 60 at all current conditions and achieved the maximum of 87 at 16 mA drive current, which was close to the commercial LED (maximum 90). Finally, the luminous intensity test under long time operation also showed that the WLED had practical application prospects. Even after 32 h of continuous operation, the luminous intensity remained above 95%, and the peak position was not significantly shifted (Figure 5D). In conclusion, the passivation strategy using highly crystalline TiO2: Eu3+ hollow shells as protective layer and emission source can expand the application of perovskite materials in optoelectronic field.

4 Conclusion

In summary, $CsPbCl_{0.3}Br_{2.7}/TiO_2:Eu^{3+}$ composites with multi-color light emission were in-situ grown with TiO2 as the protective shell and Eu3+ ions as the red light source. It was found that $TiO_2:Eu^{3+}$ hollow shells had the best red light emission and crystallinity when the Eu^{3+} doping amount was at 0.6 mmol and the annealing temperature was 800°C. Meanwhile, when the Cl^-/Br^- ratio of $CsPb(Cl/Br)_3$ NCs was 1:9, the emission peaks of NCs and Eu^{3+} had the best matching effect, resulting in pure white light emission. The stability of the $CsPbCl_{0.3}Br_{2.7}/TiO_2:Eu^{3+}$ composites was significantly improved due to the protection of the external highly crystalline $TiO_2:Eu^{3+}$ shell layer. Moreover, the WLED prepared with the materials exhibited a luminous efficiency of 87.39 lm/W and long-time operating stability. In conclusion, the highly efficient and stable white light emission by packaging $CsPb(Cl/Br)_3$ NCs in high crystallinity shells showed great potential in the field of optoelectronics.

Data availability statement

The original contributions presented in the study are included in the article/Supplementary Material, further inquiries can be directed to the corresponding author.

Author contributions

JS and JW contributed equally to this work, and their tasks is to prepare the PS film. ZD, YZ, and YX helped a lot in preparing the WLED and testing their EL abilities. NG and AB helped a lot in finally organization of the manuscript. All authors listed have made a substantial, direct, and intellectual contribution to the work and approved it for publication.

Funding

This work was supported by the National Natural Science Foundation of China (NSFC, 52161145103 and 61774124), National Key R&D Program of China (2022YFE0122500 and 2019YFB1503200), 111 Program (No. B14040), and Shaanxi Provincial Key Research and Development Program (No. 2021GXLH-Z-084).

Acknowledgments

The authors thank Ms. Dan He at Instrument Analysis Center of Xi'an Jiaotong University for her the help with the time-resolved PL analysis.

Conflict of interest

The authors declare that the research was conducted in the absence of any commercial or financial relationships that could be construed as a potential conflict of interest.

Publisher's note

Supplementary material

The Supplementary Material for this article can be found online at: https://www.frontiersin.org/articles/10.3389/fchem.2023.1199863/full#supplementary-material

References

Bae, W. K., Park, Y. S., Lim, J., Lee, D., Padilha, L. A., McDaniel, H., et al. (2013). Controlling the influence of Auger recombination on the performance of quantum-dot light-emitting diodes. *Nat. Commun.* 4, 2661. doi:10.1038/ncomms3661

Bai, Y., Hao, M., Ding, S., Chen, P., and Wang, L. (2022). Surface chemistry engineering of perovskite quantum dots: Strategies, applications, and perspectives. *Adv. Mater* 34 (4), e2105958. doi:10.1002/adma.202105958

Chang, M., Song, Y., Chen, J., Cui, L., Shi, Z., Sheng, Y., et al. (2017). Photocatalytic and photoluminescence properties of core–shell SiO_2@TiO_2:Eu^{3+},Sm^{3+} and its etching products. *ACS Sustain. Chem. Eng.* 6 (1), 223–236. doi:10.1021/acssuschemeng.7b02285

Dai, X., Zhang, Z., Jin, Y., Niu, Y., Cao, H., Liang, X., et al. (2014). Solution-processed, high-performance light-emitting diodes based on quantum dots. *Nature* 515 (7525), 96–99. doi:10.1038/nature13829

Dong, H., Kareem, S., Gong, X., Ruan, J., Gao, P., Zhou, X., et al. (2021). Water-triggered transformation of ligand-free lead halide perovskite nanocrystal-embedded Pb(OH)Br with ultrahigh stability. *ACS Appl. Mater Interfaces* 13 (20), 23960–23969. doi:10.1021/acsami.1c06627

Dong, Y., Wang, Y. K., Yuan, F., Johnston, A., Liu, Y., Ma, D., et al. (2020). Bipolar-shell resurfacing for blue LEDs based on strongly confined perovskite quantum dots. *Nat. Nanotechnol.* 15 (8), 668–674. doi:10.1038/s41565-020-0714-5

Fakharuddin, A., Qiu, W., Croes, G., Devižis, A., Gegevičius, R., Vakhnin, A., et al. (2019). Reduced efficiency roll-off and improved stability of mixed 2D/3D perovskite light emitting diodes by balancing charge injection. *Adv. Funct. Mater.* 29 (37), 1904101. doi:10.1002/adfm.201904101

Fan, M., Huang, J., Turyanska, L., Bian, Z., Wang, L., Xu, C., et al. (2023). Efficient all-perovskite white light-emitting diodes made of *in situ* grown perovskite-mesoporous silica nanocomposites. *Adv. Funct. Mater.* 2023, 2215032.

Gao, W., Ge, W., Shi, J., Tian, Y., Zhu, J., and Li, Y. (2021). Stretchable, flexible, and transparent $SrAl_2O_4$:Eu^{2+}@TPU ultraviolet stimulated anti-counterfeiting film. *Chem. Eng. J.* 405, 126949. doi:10.1016/j.cej.2020.126949

He, C., Takeda, T., Huang, Z., Xu, J., Chen, J., Yi, W., et al. (2023). Powder synthesis and luminescence of a novel yellow-emitting $Ba_5Si_{11}Al_7N_{25}$: Eu^{2+} phosphor discovered by a single-particle-diagnosis approach for warm w-LEDs. *Chem. Eng. J.* 455, 140932. doi:10.1016/j.cej.2022.140932

He, M., Zhang, Q., Carulli, F., Erroi, A., Wei, W., Kong, L., et al. (2022). Ultra-stable, solution-processable $CsPbBr_3$-SiO_2 nanospheres for highly efficient color conversion in micro light-emitting diodes. *ACS Energy Lett.* 8 (1), 151–158. doi:10.1021/acsenergylett.2c02062

Huang, C.-Y., Li, H., Wu, Y., Lin, C.-H., Guan, X., Hu, L., et al. (2022). Inorganic halide perovskite quantum dots: A versatile nanomaterial platform for electronic applications. *Nano-Micro Lett.* 15 (1), 16. doi:10.1007/s40820-022-00983-6

Ji, Y., Wang, M., Yang, Z., Qiu, H., Padhiar, M. A., Zhou, Y., et al. (2021). Trioctylphosphine-assisted pre-protection low-temperature solvothermal synthesis of highly stable $CsPbBr_3$/TiO_2 nanocomposites. *J. Phys. Chem. Lett.* 12 (15), 3786–3794. doi:10.1021/acs.jpclett.1c00693

Mrázek, J., Surýnek, M., Bakardjieva, S., Buršík, J., Proboštová, J., and Kašík, I. (2015). Luminescence properties of nanocrystalline europium titanate $Eu_2Ti_2O_7$. *J. Alloys Compd.* 645, 57–63. doi:10.1016/j.jallcom.2015.05.019

Ningthoujam, R. S., Sudarsan, V., Vatsa, R. K., Kadam, R. M., Jagannath and Gupta, A. (2009). Photoluminescence studies on Eu doped TiO_2 nanoparticles. *J. Alloys Compd.* 486 (1-2), 864–870. doi:10.1016/j.jallcom.2009.07.090

Orihashi, T., Nakamura, T., Adachi, S., and Srivastava, A. (2016). Synthesis and unique photoluminescence properties of $Eu_2Ti_2O_7$ and Eu_2TiO_5. *J. Am. Ceram. Soc.* 99 (9), 3039–3046. doi:10.1111/jace.14318

Pan, G., Bai, X., Xu, W., Chen, X., Zhou, D., Zhu, J., et al. (2018). Impurity ions codoped cesium lead halide perovskite nanocrystals with bright white light emission toward ultraviolet-white light-emitting diode. *ACS Appl. Mater Interfaces* 10 (45), 39040–39048. doi:10.1021/acsami.8b14275

Pan, G., Bai, X., Yang, D., Chen, X., Jing, P., Qu, S., et al. (2017). Doping lanthanide into perovskite nanocrystals: Highly improved and expanded optical properties. *Nano Lett.* 17 (12), 8005–8011. doi:10.1021/acs.nanolett.7b04575

Pan, J., Quan, L. N., Zhao, Y., Peng, W., Murali, B., Sarmah, S. P., et al. (2016). Highly efficient perovskite-quantum-dot light-emitting diodes by surface engineering. *Adv. Mater* 28 (39), 8718–8725. doi:10.1002/adma.201600784

Pan, J., Shang, Y., Yin, J., De Bastiani, M., Peng, W., Dursun, I., et al. (2018). Bidentate ligand-passivated $CsPbI_3$ perovskite nanocrystals for stable near-unity photoluminescence quantum yield and efficient red light-emitting diodes. *J. Am. Chem. Soc.* 140 (2), 562–565. doi:10.1021/jacs.7b10647

Protesescu, L., Yakunin, S., Bodnarchuk, M. I., Krieg, F., Caputo, R., Hendon, C. H., et al. (2015). Nanocrystals of cesium lead halide perovskites ($CsPbX_3$, X = Cl, Br, and I): Novel optoelectronic materials showing bright emission with wide color gamut. *Nano Lett.* 15 (6), 3692–3696. doi:10.1021/nl5048779

Ravi, V. K., Saikia, S., Yadav, S., Nawale, V. V., and Nag, A. (2020). $CsPbBr_3$/ZnS core/shell type nanocrystals for enhancing luminescence lifetime and water stability. *ACS Energy Lett.* 5 (6), 1794–1796. doi:10.1021/acsenergylett.0c00858

Reszczyńska, J., Grzyb, T., Wei, Z., Klein, M., Kowalska, E., Ohtani, B., et al. (2016). Photocatalytic activity and luminescence properties of RE^{3+}–TiO_2 nanocrystals prepared by sol–gel and hydrothermal methods. *Appl. Catal. B Environ.* 181, 825–837. doi:10.1016/j.apcatb.2015.09.001

Shi, J., Ge, W., Gao, W., Xu, M., Zhu, J., and Li, Y. (2019). Enhanced thermal stability of halide perovskite $CsPbX_3$ nanocrystals by a facile TPU encapsulation. *Adv. Opt. Mater.* 8 (4), 1901516. doi:10.1002/adom.201901516

Shi, J., Ge, W., Tian, Y., Xu, M., Gao, W., and Wu, Y. (2021). Enhanced stability of all-inorganic perovskite light-emitting diodes by a facile liquid annealing strategy. *Small* 17 (14), e2006568. doi:10.1002/smll.202006568

Shi, J., Ge, W., Zhu, J., Saruyama, M., and Teranishi, T. (2020). Core–shell $CsPbBr_3$@CdS quantum dots with enhanced stability and photoluminescence quantum yields for optoelectronic devices. *ACS Appl. Nano Mater.* 3 (8), 7563–7571. doi:10.1021/acsanm.0c01204

Shi, J., Wang, M., Wang, H., Zhang, C., Ji, Y., Wang, J., et al. (2022). Preparation of ultra-stable and environmentally friendly $CsPbBr_3$@ZrO_2/PS composite films for white light-emitting diodes. *Nanoscale* 14 (44), 16548–16559. doi:10.1039/d2nr04255j

Song, J., Li, J., Li, X., Xu, L., Dong, Y., and Zeng, H. (2015). Quantum dot light-emitting diodes based on inorganic perovskite cesium lead halides ($CsPbX_3$). *Adv. Mater* 27 (44), 7162–7167. doi:10.1002/adma.201502567

Tang, X., Zu, Z., Shao, H., Hu, W., Zhou, M., Deng, M., et al. (2016). All-inorganic perovskite $CsPb(Br/I)_3$ nanorods for optoelectronic application. *Nanoscale* 8 (33), 15158–15161. doi:10.1039/c6nr01828a

Wang, S., Xu, J., Wang, J., Wang, K.-Y., Dang, S., Song, S., et al. (2017). Luminescence of samarium(iii) bis-dithiocarbamate frameworks: Codoped lanthanide emitters that cover visible and near-infrared domains. *J. Mater. Chem. C* 5 (26), 6620–6628. doi:10.1039/c7tc01844d

Werts, M. H. V., Jukes, R. T. F., and Verhoeven, J. W. (2002). The emission spectrum and the radiative lifetime of Eu^{3+} in luminescent lanthanide complexes. *Phys. Chem. Chem. Phys.* 4 (9), 1542–1548. doi:10.1039/b107770h

Xu, J., Huang, X., Cheng, X., Whangbo, M. H., and Deng, S. (2022). Microscopic mechanism of the heat-induced blueshift in phosphors and a logarithmic energy dependence on the nearest dopant-vacancy distance. *Angew. Chem. Int. Ed. Engl.* 61 (15), e202116404. doi:10.1002/anie.202116404

Yan, D., Zhao, S., Wang, H., and Zang, Z. (2020). Ultrapure and highly efficient green light emitting devices based on ligand-modified $CsPbBr_3$ quantum dots. *Photonics Res.* 8 (7), 1086. doi:10.1364/prj.391703

Yang, D., Li, P., Zou, Y., Cao, M., Hu, H., Zhong, Q., et al. (2019). Interfacial synthesis of monodisperse $CsPbBr_3$ nanorods with tunable aspect ratio and clean surface for efficient light-emitting diode applications. *Chem. Mater.* 31 (5), 1575–1583. doi:10.1021/acs.chemmater.8b04651

Yang, X., Ma, L., Li, L., Luo, M., Wang, X., Gong, Q., et al. (2023). Towards micro-PeLED displays. *Nat. Rev. Mater.* 8, 341–353. doi:10.1038/s41578-022-00522-0

Yang, Y., Zheng, Y., Cao, W., Titov, A., Hyvonen, J., Manders, J. R., et al. (2015). High-efficiency light-emitting devices based on quantum dots with tailored nanostructures. *Nat. Photonics* 9 (4), 259–266. doi:10.1038/nphoton.2015.36

Yoon, S., Seo, M., Kim, I. S., Lee, K., and Woo, K. (2023). Ultra-stable and highly efficient white light emitting diodes through CsPbBr(3) perovskite nanocrystals-silica composite phosphor functionalized with surface phenyl molecules. *Small* 19 (7), e2206311. doi:10.1002/smll.202206311

Yuan, L., Zhou, L., Xiang, W., and Liang, X. (2020). Enhanced stability of red-emitting $CsPbI_3$:Yb^{3+} nanocrystal glasses: A potential luminescent material. *J. Non-Crystalline Solids* 545, 120232. doi:10.1016/j.jnoncrysol.2020.120232

Zhang, A., Dong, C., and Ren, J. (2017). Tuning blinking behavior of highly luminescent cesium lead halide nanocrystals through varying halide composition. *J. Phys. Chem. C* 121 (24), 13314–13323. doi:10.1021/acs.jpcc.7b00343

Zhou, J., Huang, F., Lin, H., Lin, Z., Xu, J., and Wang, Y. (2016). Inorganic halide perovskite quantum dot modified YAG-based white LEDs with superior performance. *J. Mater. Chem. C* 4 (32), 7601–7606. doi:10.1039/c6tc02405j